Special Report
National Aeronautics and Space Administration
Langley Research Center
Grant NGR 23-004-091

THE USE OF DIGITAL TECHNIQUES TO EXAMINE THE INTERMITTENT REGION OF A TURBULENT JET

prepared by

John F. Foss
Thomas E. Merrow

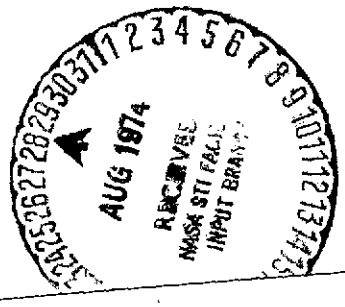

Division of Engineering Research
MICHIGAN STATE UNIVERSITY
East Lansing, Michigan 48824
August 15, 1974

Special Report
National Aeronautics and Space Administration
Langley Research Center
Grant NGR 23-004-091

THE USE OF DIGITAL TECHNIQUES TO EXAMINE THE INTERMITTENT REGION OF A TURBULENT JET

prepared by

John F. Foss
Thomas E. Merrow

Division of Engineering Research
MICHIGAN STATE UNIVERSITY
East Lansing, Michigan 48824
August 15, 1974

ABSTRACT

Voltage signals, sampled at a high rate in the intermittent region of a round jet, are analyzed to provide instantaneous velocity vector information and measures of the vorticity and dissipation scales.

A clustering routine to assess the feasibility of using the voltage readings to define the vortical, nonvortical state of the flow is also utilized. The results indicate that the clustering routine is partially successful; more sophisticated discrimination techniques will be required for a complete specification.

FORWORD

This report, submitted in conjunction with NASA Grant NGR 23-004-091, was initiated as an ME 499 project by Mr. Thomas Merrow under the direction of the senior author. Its relationship to the vorticity measurements to be executed in conjunction with this grant and the general importance of intermittency in aerodynamic noise generation prompts its inclusion in the series of reports associated with this grant. Mr. Merrow's interest in pattern recognition was developed through independent study under the direction of Professor Richard C. Dubes of the Computer Science Department at Michigan State University. This study, conducted as a part of his academic program, complemented his fifteen-month work experience during which he made numerous major and specific contributions to our digital data acquisition and experimental control capability.

1. INTRODUCTION

A turbulent flow which is exposed to ambient fluid is bounded by a thin, highly convoluted surface which has been termed "the viscous superlayer" (see Figure 1). Vorticity and vorticity fluctuations are diffused into the ambient fluid at this interface; i.e., the interface propagates outward with respect to the fluid which previously contained it. The interface is maintained as a sharp front as a result of the gradient steepening effects of the small scale turbulent motions.

At a given point in space, the fliud elements may be characterized as either vortical or nonvortical depending upon whether the point is interior or exterior (respectively) with respect to this interface. Since this surface is corrugated by the large scale turbulent motions, the conditions at a given point can vary quite rapidly in time as the superlayer is convected past the point. Vorticity, $\underset{\sim}{\omega}$, is a vector point function and is defined as

$$\underset{\sim}{\omega} \equiv \nabla \times \underset{\sim}{v}. \tag{1}$$

Because $\underset{\sim}{\omega}$ involves derivatives of the velocity field it is quite difficult to measure and, consequently, it is quite unsatisfactory to use a direct approach in the experimental definition of the vortical, nonvortical condition. However, it is experimentally feasible to isolate a portion of the azimuthal ϕ vorticity component using an x-array hot-wire probe. Namely, from

$$\omega_\phi = \frac{\partial u}{\partial r} - \frac{\partial v}{\partial x} \tag{2}$$

and using the x-wire to isolate v(t), the $\partial v/\partial x$ term can be approximated as

$$-\frac{\partial v}{\partial x} \simeq \frac{1}{u}\frac{\partial v}{\partial t}. \tag{3}$$

Similarly, two parallel straight wires could be used to approximate $\partial u/\partial y$. Unfortunately, the combination of these probe arrays would be quite large with respect to the dimensions of the interface.

Some form of analog signal processing characterizes nearly all of the discrimination techniques to distinguish the vortical, nonvortical condition. It was the purpose of the present study to determine if this binary condition could be directly inferred from the state of the unprocessed hot-wire voltage signals. The advantages of such a discrimination are obvious from the standpoint of an on-line signal processing capability. The likelihood

that such a scheme is feasible is predicated upon the different states of the flow as the vortical or nonvortical fluid occupies the measuring point. Specifically, it can be anticipated that the velocity magnitude is larger and the velocity direction is close to the streaming flow direction when vortical fluid is present. Conversely, and on the average, the velocity magnitude is less and the velocity vector is directed toward the jet axis when nonvortical fluid is present.

2. DATA CHARACTERISTICS AND DATA PROCESSING

The data base for the present study was collected at approximately three diameters downstream from the exit of an axisymmetric jet. Linearized hot-wire channels were used to form the wire 1, wire 2 voltages (E_1, E_2) used extensively herein. The probe axis was aligned parallel to the axis of the jet. The three data sets are representative of jet locations at which large, medium, and small intermittency γ values can be expected. ($\gamma \equiv$ percent time that vortical fluid occupies the measuring locations.)

Each data set was obtained using the acquisition process summarized in Figure 2. The Texas Instruments 960A minicomputer was used to drive a four-channel A-D conversion system using the algorithm flow charted in Figure 2. In order to adequately describe the physical phenomena, the data acquisition system was designed to read at the maximum possible rate. A read rate per channel of 15.4KHz was obtained and thus the data represents sets of four measurements taken at 260 μs intervals. The two wire readings were in adjacent channels on the A-D converter and were read 65 μs apart. There was no delay between sets of measurements.

The 12-bit output from the A-D converter was processed into a voltage by (1) floating the 12-bit value to form a floating point number between -2047 and +2047 and (2) dividing the floating point number by a standardization value associated with the channel used. The standardization values are formed by employing step (1) above with a 12-bit number read when 1 volt was the input. Discrimination of about .01 volts was possible with this system.

The first data set consists of 500 of the subsets of four measurements read in a flow with a large intermittency value. The second data set is composed of 448 readings for a medium intermittency condition, and the third set consists of 448 readings in a low intermittency condition.

The instantaneous velocity vector is of principal interest in this study. Digital determination of this vector is possible from the observed voltages E_1 and E_2 read at each point. A calibration table relating voltage to velocity was obtained for each wire with the x-wire shaft parallel to the low turbulence level jet core flow used for the calibrating air flow. For simplicity, a cosine response to a yawed velocity vector is assumed for the calculations. The data acquisition system allowed the evaluation of this assumption; it was shown to be quite satisfactory for angles within $\simeq \pm 20$ degrees of the head on condition, i.e., up to 65 degrees of yaw with respect to the wire.

Since the two wires are at right angles to each other, the response of each may be expressed as

$$E_1 = E_o)_1 \cos (T + \pi/4) \tag{4}$$

$$E_2 = E_o)_2 \cos (T - \pi/4) \tag{5}$$

where T is the angle between the flow direction and the bisector of the two wires. $E_o)_1$ and $E_o)_2$ represent the response of the hot wires for $T = 0$; specifically

$$E_o)_1 = f(V) \tag{6}$$

$$E_o)_2 = g(V) \tag{7}$$

and

$$E_1 = f(V) \cos (T + \pi/4) \tag{8}$$

$$E_2 = g(V) \cos (T - \pi/4) . \tag{9}$$

Therefore, for a given E_1 and E_2 and definition of f and g through a calibration table, it is possible to determine V and T to obtain the velocity vector associated with the reading. The unique pairing of a set (E_1, E_2) to a set (V, T) is a result of the cosine assumption. Figure 3 illustrates the principles involved. The determination is made through an iterative scheme. An initial estimate of the interval which contains the actual velocity is made. The end points of the interval are found by assuming that E_1 and E_2 represent voltage readings for $T = 0$. Thus,

$$V_1 = f^{-1}(E_1) \tag{10}$$

$$V_2 = g^{-1}(E_2) \tag{11}$$

and V_{min} is the minimum of V_1 and V_2, V_{max} the maximum. This is shown in Figure 4.

Each iteration involves examining the interval $[V_{min}, V_{max}]$ by bisection into $[V_{min}, V_{mid}]$ and $[V_{mid}, V_{max}]$. Using V_{mid} and E_1, T_c may be calculated by

$$T_c = \cos^{-1}(E_1/f(V_{mid})) - \pi/4 . \tag{12}$$

Using this T_c and E_2, a new velocity, V_{cal}, may be found by

$$V_{cal} = g^{-1}(E_2 \cos(T_c - \pi/4)) . \tag{13}$$

If V_{cal} is in the interval $[V_{min}, V_{mid}]$ then the actual velocity V must also be. Similarly, if V_{cal} is in the interval $[V_{mid}, V_{max}]$ then V also falls within this region. This process is shown in Figure 5. Each iteration thus makes use of a new interval that is both half the size of the former and contains V. Iterations may be continued until the error, i.e., the size of the interval, becomes satisfactorily small.

Each reading was processed in this manner and the various sets of data analyzed visually by plotting of the velocity vectors. These velocity vector plots are constructed with fifty readings to a line and are read from left to right and top to bottom (see Figures 6 through 8).

3. DATA ANALYSIS BY CLUSTERING ALGORITHMS

As noted earlier, the development of vortical, nonvortical discrimination capability based upon the x-wire voltage would be most advantageous. Specifically, data acquisition--the long process of computing vectors for each reading--is not practical, and working with calibration tables to obtain velocities has similar disadvantages.

Since voltages have little meaning except as interpreted through calibration tables and as relative quantities, a scheme utilizing scaling values was needed to allow comparision of different data sets. Normalization of the velocity values by subtracting the mean and dividing by the standard deviation of the distribution of voltages was performed on each data set. This is shown on the E_1, E_2 data plots of Figures 9 through 11.

Each normalized data set was then analyzed using a clustering algorithm named CLUSTER.* CLUSTER searches through the readings

*Available under this designation at the MSU Computer Center. Contact the senior author to obtain a listing of the program.

and labels each one in such a way that all readings with the same label are "close" to each other. The number of clusters is specified for each run of the program. Closeness is defined through squared error. The squared deviation of a group of readings with the same label (i.e., a cluster) is the total squared distance from each point to the centroid of the cluster. The result is a set of clusters with minimum squared deviation in the sense that relabeling any reading will not reduce the total squared deviation.

The output of CLUSTER is summarized in two ways. First, the cluster centers are superimposed on the plots of the readings of E_1 versus E_2 in Figures 9 through 11. Second, the outputs from the routine are presented in Tables 2 through 4.

4. INTERPRETATION AND DISCUSSION OF RESULTS

4.1. Data Acquisition Rate

A certain concern in the present experiments is whether the maximum possible reading rate is sufficient to adequately track the details of interest. In order to assess this, two characteristic times can be examined; both times have the general character of an appropriate length divided by the mean streamwise velocity of the flow. That is, this measure represents the rate at which the turbulence structure characterized by the length is convected past the probe.

The Kolmogoroff scale η* can be calculated from the dissipation rate and the viscosity, viz.,

$$\eta = [\nu^3/\epsilon]^{1/4} \tag{14}$$

where ϵ (the dissipation rate) will be approximated as

$$\epsilon \approx 15\nu\, u^2/\lambda_f^2 \tag{15}$$

and the Taylor microscale λ_f is given by the following expression

$$\lambda_f = \overline{u^2}/\overline{\left(\frac{\partial u}{\partial x}\right)^2}\,. \tag{16}$$

The results of this calculation are shown in Table 5.

The second length scale of interest is that of the Taylor microscale

*η can be interpreted as a measure of the smallest, dynamically significant scales in a turbulent motion. The maximum dissipation rate for locally isotropic turbulence occurs at a wave number of $\simeq 0.2\,\eta$.

since this is an approximation of a typical length scale for the vorticity in the flow. The results of this calculation [see equation (16)] are also presented in Table 5.

From Table 5 it is apparent that the time resolution is quite inadequate to resolve the passage of the interface itself (since its thickness is of the order of the Kolmogoroff scale). However, the time resolution is adequate to define the velocity derivatives and to render a sufficiently "continuous" variation of the velocity field as demonstrated by Figures 6 through 8.

4.2. Interpretation of the Clustering Results

A cursory examination of Figures 6 through 11 reveals that neither the velocity vectors nor the voltage pairs will yield an obvious identification of the interface passage. This indicates that the nonvortical fluid is strongly affected by the pressure fields of the large superlayer bulges and is not "suddenly sheared" by the superlayer boundary itself.

Given these results, it was suspected that a clustering algorithm would not be able to distinguish the states of the flow based upon the voltage pairs. However, the clustering routine has been surprisingly successful; the basis for this assessment is presented below.

By the nature of the conditions within the viscous superlayer, the lateral and longitudinal velocities are correlated; hence the vortical domain on the E_1, E_2 plane is not circular but of a more general "ellipsiodal" shape. (The implied correlation between E_1 and E_2 is a result of the Reynolds "stress" effect on the mean velocity field set up by the turbulence fluctuation velocities; i.e., $\tau_{xr} = -\rho \overline{\dot{u}_x \dot{v}_r}$.) The turbulent shear stress in the nonvortical fluid is zero; hence, the nonvortical cluster for E_1, E_2 is a circular region. Secondly, since the velocity of the nonvortical fluid is, on the average, less than that of the vortical fluid, the E_1, E_2 nonvortical voltage pairs should be found at small E_1, E_2 values. These two arguments suggest that the first cluster identified by the routine is the most probable candidate for the nonvortical condition. All of the remaining clusters represent the vortical condition and the multiple circular clusters are "required" to describe the "ellipsoidal" shape.

This hypothesis is suggested by the "patterns" of Tables 2 through 4 in which an increase in the number of clusters tends to preserve the characteristics of the first one. Note that in Table 3 the proper number

of clusters for data set 2 appears to be 3 or 4; the 5 cluster configuration seems to relegate too little of the space to the nonvortical condition.

For the purpose of this study, it was desired to obtain a reference for the vortical, nonvortical condition. The quantity used was the first time derivative of the difference signal. As shown by equation (3), this is proportional to one element of the azimuthal vorticity. An approximate intermittency value may be calculated by isolating those regions where this value is relatively large. Three photographs of the scope trace of this signal along with the timing signal for the data acquisition are shown in Figure 12. Also shown are the transition points between the vortical and nonvortical condition as assessed from the clustering routine. The apparent agreement is encouraging. Intermittency values from both techniques are presented in Table 6. It is not possible to ascribe a high degree of accuracy to γ determined from the photographs. The ambiguity in the vortical, nonvortical interface is rather large although the presence of two discrete states is quite evident. A more precise definition of γ is suggested for future studies. Also, it is interesting to note that for the relatively short time of the data sample (1.3 msec), the calculated γ values for data sets 2 and 3 are approximately the same although their long-term average values are much different.

5. SUMMARY AND CONCLUSIONS

The a priori hypothesis that the instantaneous velocity vectors in the vortical and nonvortical regions of the jet would be strikingly different was proved invalid by this study. However, the ability to discriminate between these two states of the flow based upon the voltage pair from an appropriately oriented x-wire probe, a scheme which was predicated upon this hypothesis, has shown some success. It is a summary conclusion from this study that certain values of the voltage pair could be used as a sufficiency condition for the discrimination with a more sophisticated interpretation scheme for the remaining states. More specifically, for sufficiently large E_1, E_2 values, the flow state is clearly vortical; similarly, a clearly nonvortical state can be identified. However, the two conditions can clearly be expected to overlap each other in terms of their E_1, E_2 voltage pairs.

The present study will provide the basis for future and more sophisticated discrimination techniques.

Table 1. Summary of Velocity and Velocity Derivatives Information

	1		2		3	
	μ	σ	μ	σ	μ	σ
V(fps)	-1.18	6.68	-.16	5.58	.73	3.15
U(fps)	38.29	11.21	28.85	9.30	16.97	5.94
DU/DX(sec^{-1})	.127	292	.123	291	.073	222
DV/DX(sec^{-1})	-.010	260	.024	198	.005	158

Note: μ = mean, σ = standard deviation

Table 2. Clustering Results, Data Set 1

No. of Clusters	N (No. of entries in cluster)	Cluster Centers $(\tilde{E}_1 - \bar{E}_1)$, $(\tilde{E}_2 - \bar{E}_2)$	R	Designation on Figure 9
2	246	-0.572, -0.296	0.505	A 1
	254	+0.554, +0.286	0.557	A 2
3	153	-0.808, -0.422	0.406	B 1
	107	1.02, 0.479	0.370	B 2
	240	0.060, 0.056	0.396	B 3
4	84	-0.991, -0.602	0.316	C 1
	104	1.033, 0.485	0.362	C 2
	179	0.181, 0.110	0.360	C 3
	133	-0.425, -0.147	0.322	C 4
5	89	-0.953, -0.611	0.324	D 1
	104	1.033, 0.485	0.362	D 2
	111	0.119, 0.294	0.287	D 3
	100	-0.511, -0.086	0.273	D 4
	96	0.160, -0.208	0.298	D 5

Note: $\bar{E}_1$, $\bar{E}_2$ are the locations of the average voltages for the complete data sample.

$\tilde{E}_1$, $\tilde{E}_2$ are the locations of the average voltages for the cluster.

R is a measure of the average distance from the cluster center to the points in the cluster; i.e.,

$$\left\{ \sum_{j=1}^{N} \left[(E_{1j} - \tilde{E}_1)^2 + (E_{2j} - \tilde{E}_2)^2 \right] / N \right\}^{1/2}$$

Table 3. Clustering Results, Data Set 2

No. of Clusters	N (No. of entries in cluster)	Cluster Centers $(\tilde{E}_1 - \bar{E}_1)$, $(\tilde{E}_2 - \bar{E}_2)$	R	Designation on Figure 10
2	276	-0.399, -0.159	0.362	A 1
	172	0.640, +0.256	0.575	A 2
3	219	-0.494, -0.218	0.293	B 1
	56	1.23, 0.494	0.489	B 2
	173	0.229, 0.117	0.342	B 3
4	207	-0.513, 0.227	0.283	C 1
	34	1.48, 0.468	0.406	C 2
	131	0.083, 0.039	0.288	C 3
	76	0.590, 0.342	0.341	C 4
5	103	-0.635, -0.370	0.214	D 1
	33	1.498, 0.45	0.389	D 2
	115	0.218, 0.147	0.278	D 3
	60	0.615, 0.445	0.341	D 4
	137	-0.336, -0.037	0.239	D 5

Note: $\bar{E}_1$, $\bar{E}_2$ are the locations of the average voltages for the complete data samples.

$\tilde{E}_1$, $\tilde{E}_2$ are the locations of the average voltages for the cluster.

R is a measure of the average distance from the cluster center to the points in the cluster; i.e.,

$$\left\{ \sum_{j=1}^{N} [(E_{1j} - \tilde{E}_1)^2 + (E_{2j} - \tilde{E}_2)^2]/N \right\}^{1/2}$$

Table 4. Clustering Results, Data Set 3

No. of Clusters	N (No. of entries in cluster)	Cluster Centers $(\tilde{E}_1 - \overline{E}_1)$, $(\tilde{E}_2 - \overline{E}_2)$	R	Designation on Figure 11
2	306	-0.243, -0.169	0.196	A 1
	142	0.522, 0.364	0.371	A 2
3	284	-0.263, -0.192	0.157	B 1
	70	0.779, 0.494	0.273	B 2
	94	0.213, 0.213	0.235	B 3
4	220	-0.300, -0.240	0.087	C 1
	66	0.796, 0.499	0.270	C 2
	80	0.279, 0.236	0.212	C 3
	82	-0.108, 0.012	0.195	C 4
5	220	-0.300, -0.240	0.087	D 1
	41	0.898, 0.566	0.227	D 2
	61	0.175, 0.201	0.183	D 3
	53	0.529, 0.326	0.226	D 4
	73	-0.130, 0	0.181	D 5

Note: $\overline{E}_1$, $\overline{E}_2$ are the locations of the average voltages for the complete data samples.

$\tilde{E}_1$, $\tilde{E}_2$ are the locations of the average voltages for the cluster.

R is a measure of the average distance from the cluster center to the points in the cluster; i.e.,

$$\left\{ \sum_{j=1}^{N} \left[(E_{1j} - \tilde{E}_1)^2 + (E_{2j} - \tilde{E}_2)^2 \right] / N \right\}^{1/2}$$

Table 5. Characteristic Lengths and Times to Estimate the Adequacy of the 65 μsec Delay in the Construction of $\underset{\sim}{V}(x, r, t)$

Data Set No.	$\eta = [\nu^3/\epsilon]^{1/4}$ (ft) x 10^{-4}	$\lambda_f = \left[\overline{u^2}/\overline{\left(\frac{\partial u}{\partial x}\right)^2}\right]^{1/2}$ (ft) x 10^{-2}	$\eta/\bar{u}$ (sec) 10^{-6}	$\lambda_f/\bar{u}$ (sec) 10^{-6}
1	3.67	3.87	9.6	1000
2	3.67	3.18	12.8	1100
3	4.22	2.65	25	1560

To allow direct comparison to 65 μsec time between the individual readings, sec x 10^{-6} velocity derivatives are formed over a time scale of 260 μsec.

Table 6. Intermittency Values Obtained from the Signal $\partial(E_1 - E_2)/\partial t$ and from the Clustering Algorithm

	1	2	3
γ photo	81	59	47
γ cluster	82	54	51

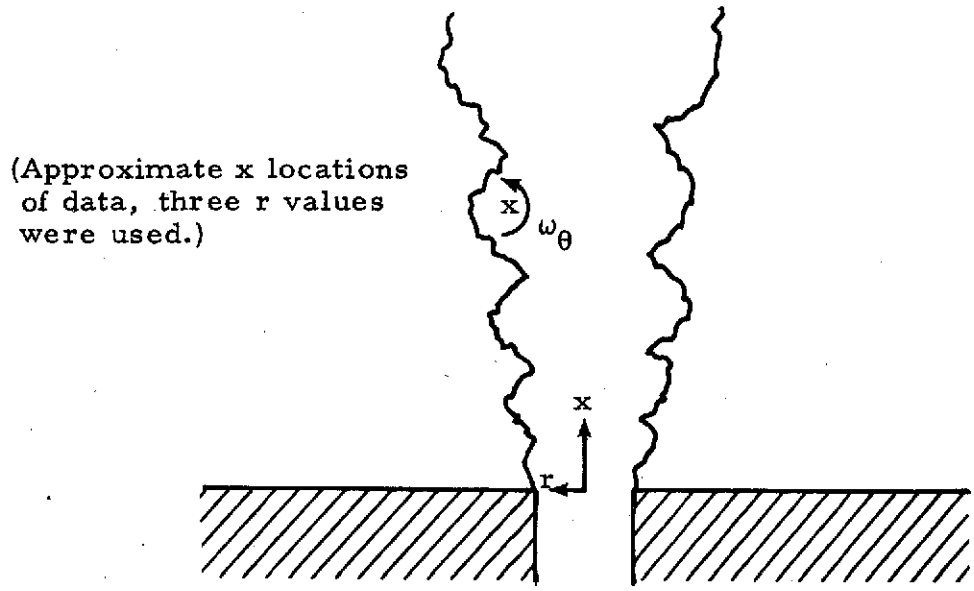

Figure 1. Schematic of viscous superlayer and terms used in the description of this investigation.

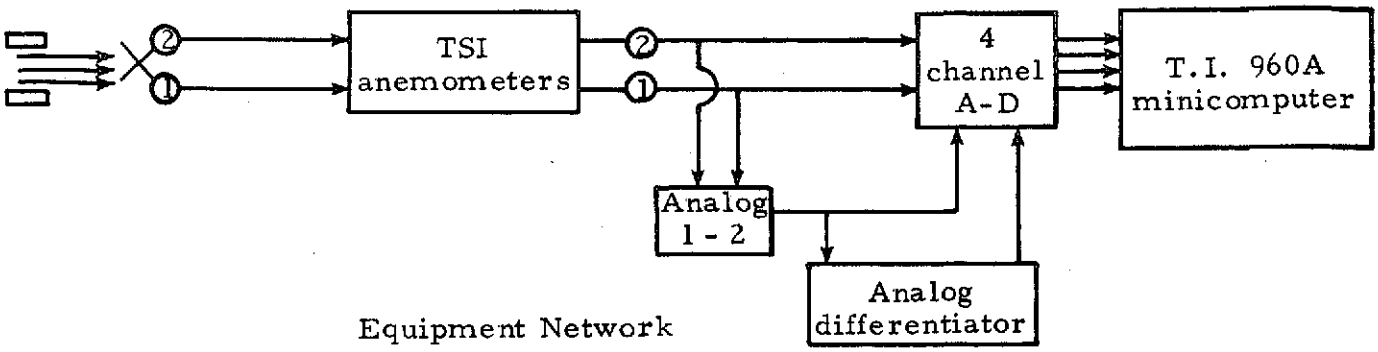

Equipment Network

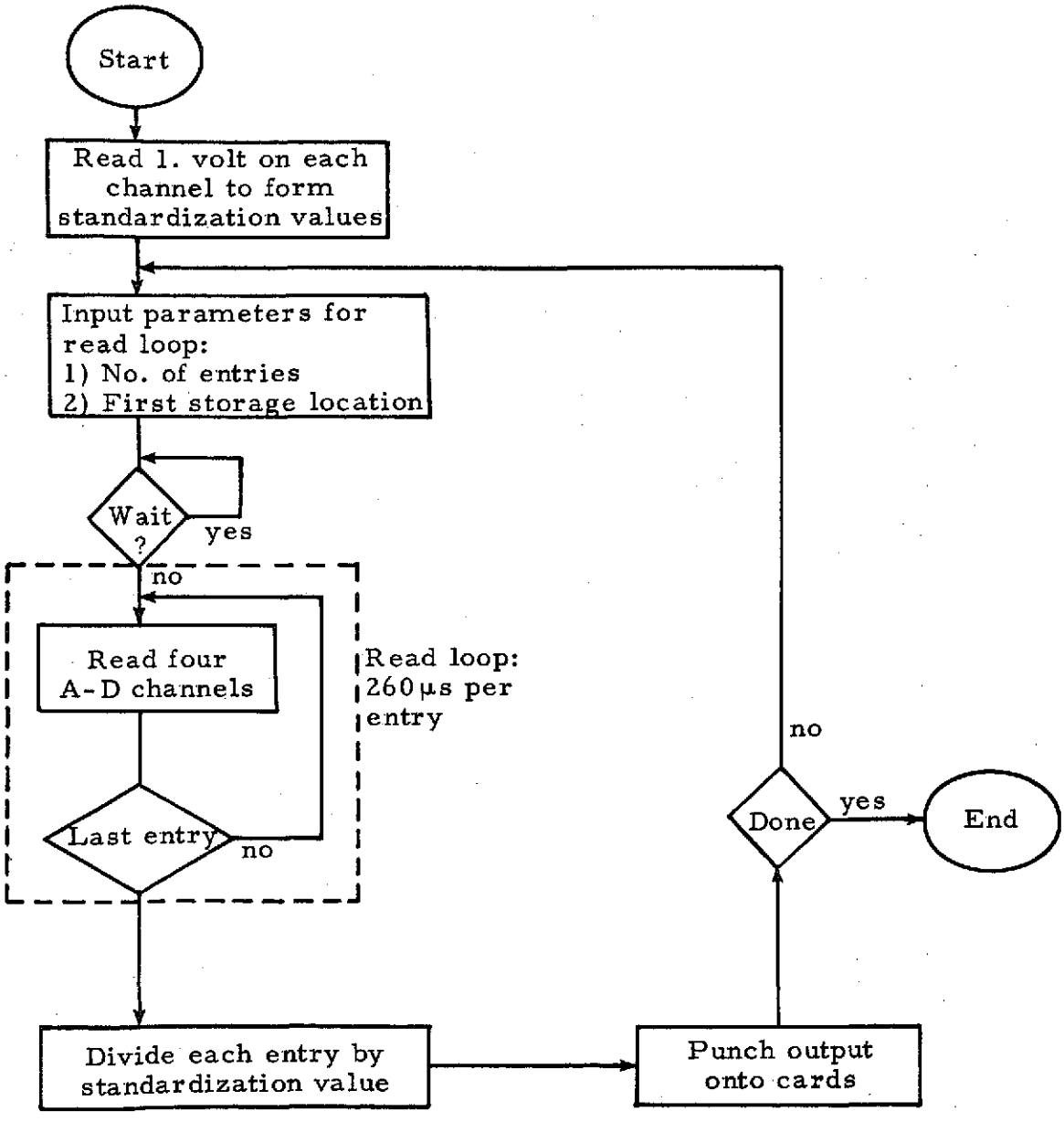

Figure 2. Schematic representation of the data acquisition system.

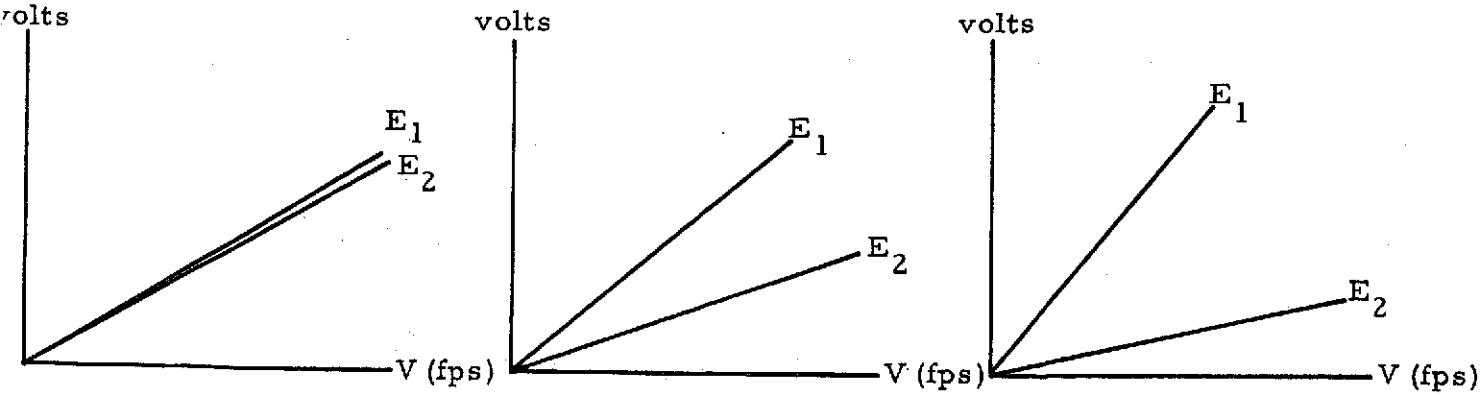

a) Calibration, T = 0 degrees

b) Calibration, T = 15 degrees

c) Calibration, T = 30 degrees

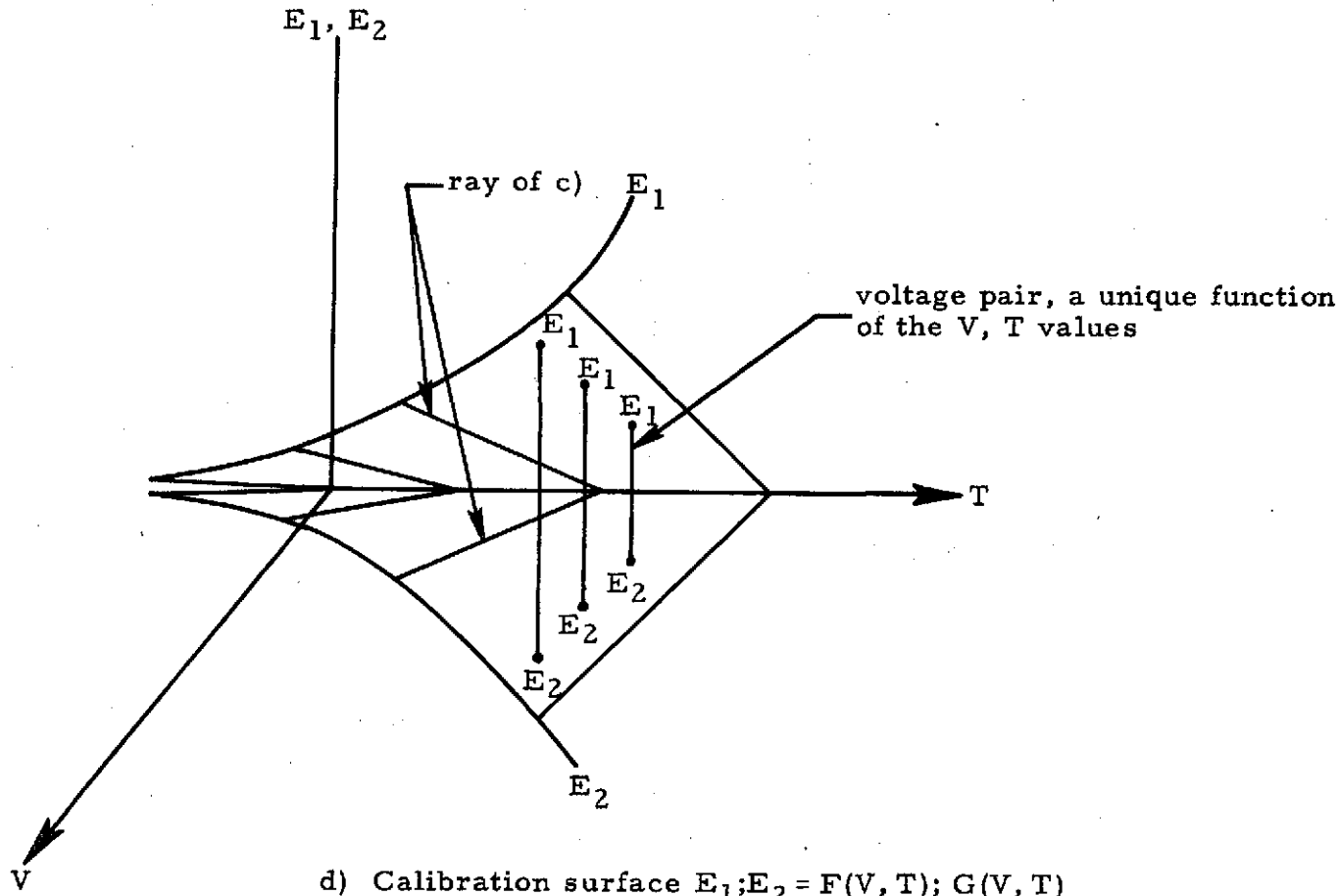

d) Calibration surface $E_1; E_2 = F(V, T); G(V, T)$
(Note: Calibration surface extends to $T < 0$ and is an add function of T)

Figure 3. Schematic of calibration data.

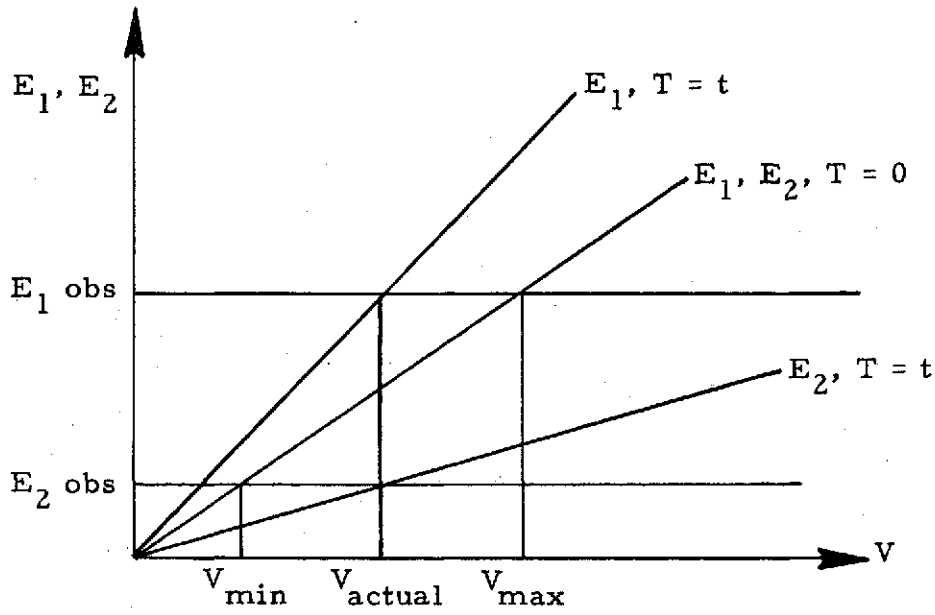

(Note: V_{actual} is the true magnitude, t is the true direction of vector)

Figure 4. Definition of terms used in the velocity calculation scheme.

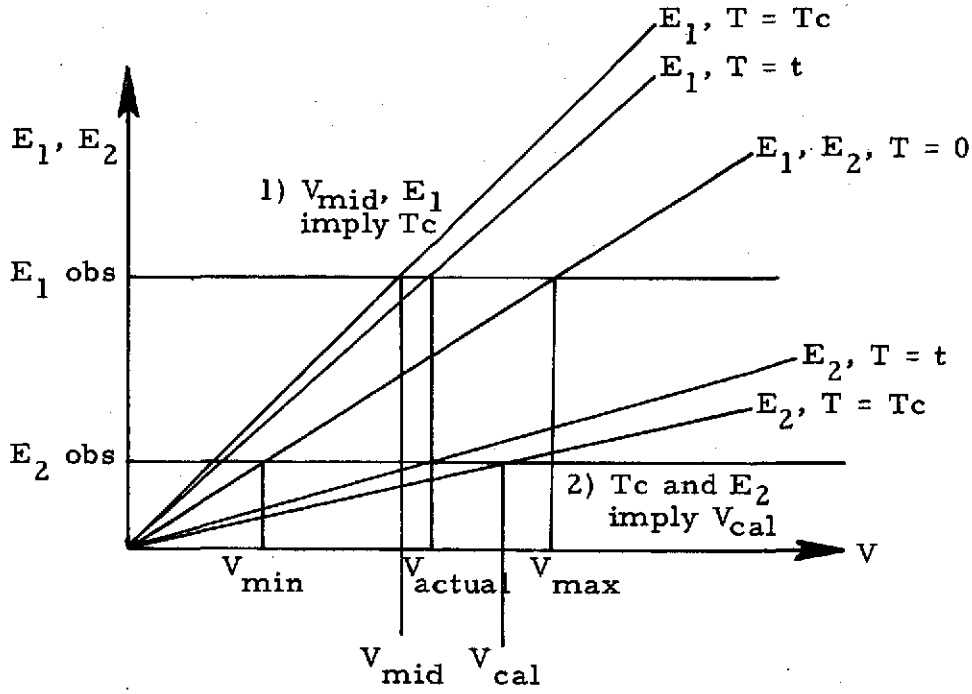

Figure 5. Schematic representation of two iterations in the velocity calculation scheme.

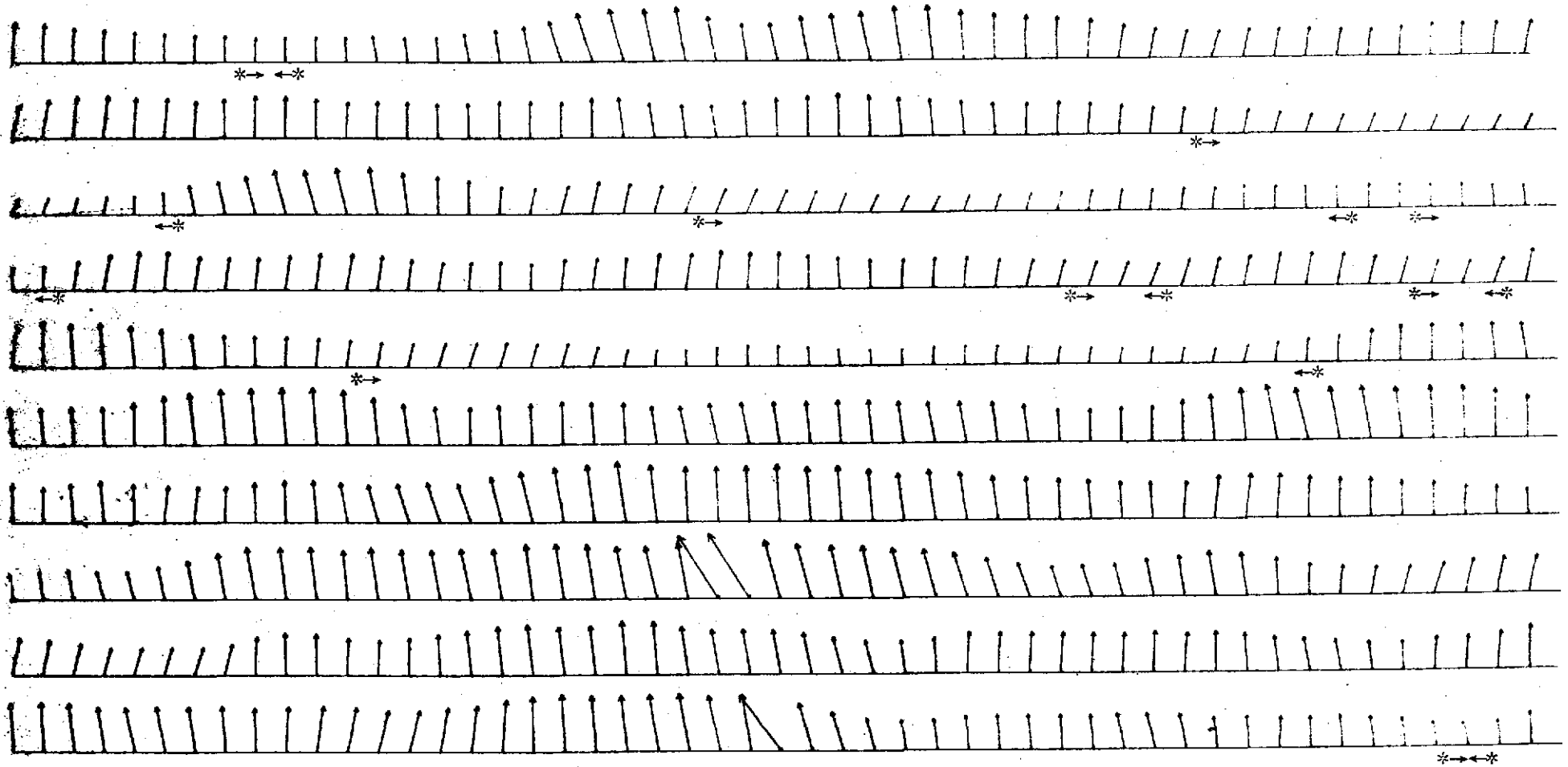

Figure 6. Velocity Vectors for Data Set 1

Note: Each vector is calculated from a pair of voltage readings separated by 65 μsec. There are 260 μsec between each vector. See Table 1 for the statistical evaluation of these data.
Note: The interval designated "1" or "nonvortical" by the appropriate clustering routine is shown by the symbols *→ ←*.

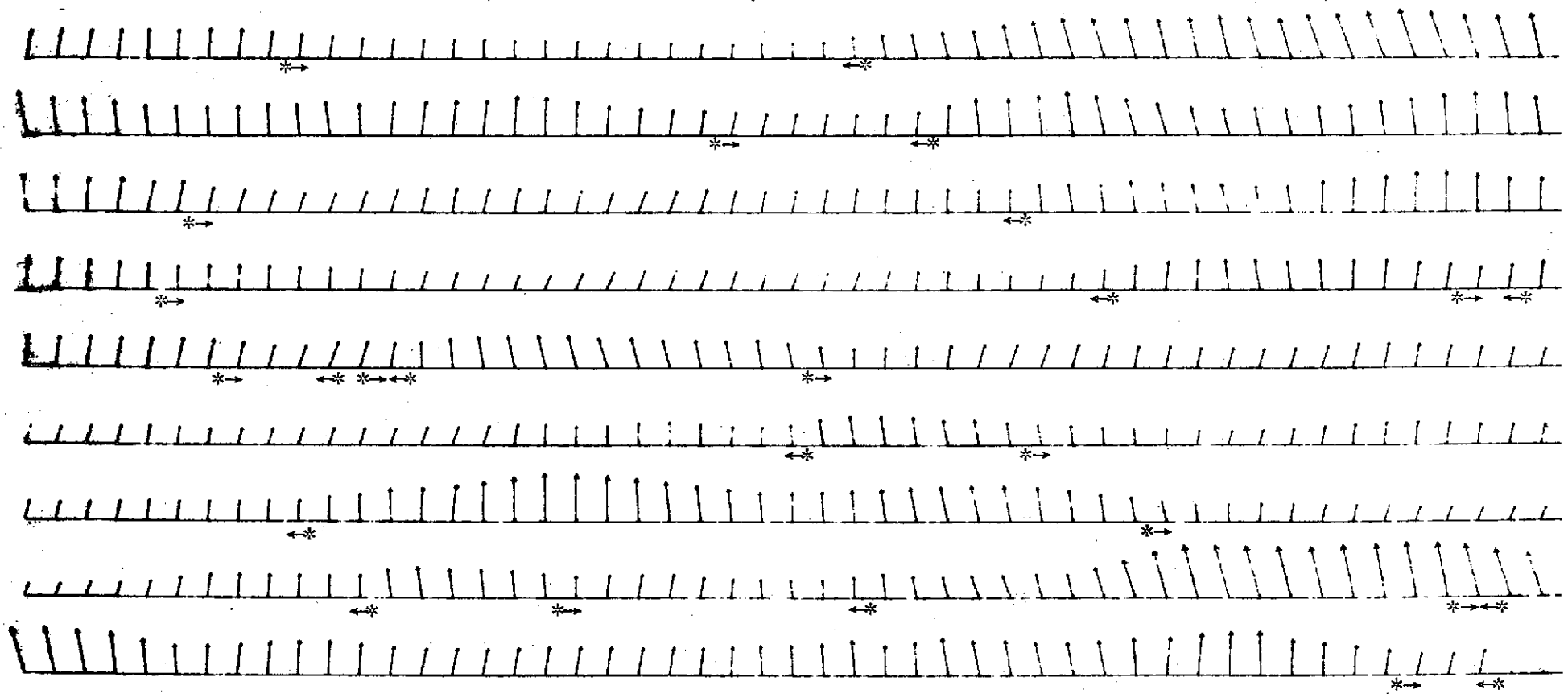

Figure 7. Velocity Vectors for Data Set 2

Note: Each vector is calculated from a pair of voltage readings separated by 65 μsec. There are 260 μsec between each vector. See Table 1 for the statistical evaluation of these data.

Note: The interval designated "1" or "nonvortical" by the appropriate clustering routine is shown by the symbols *→ ←*.

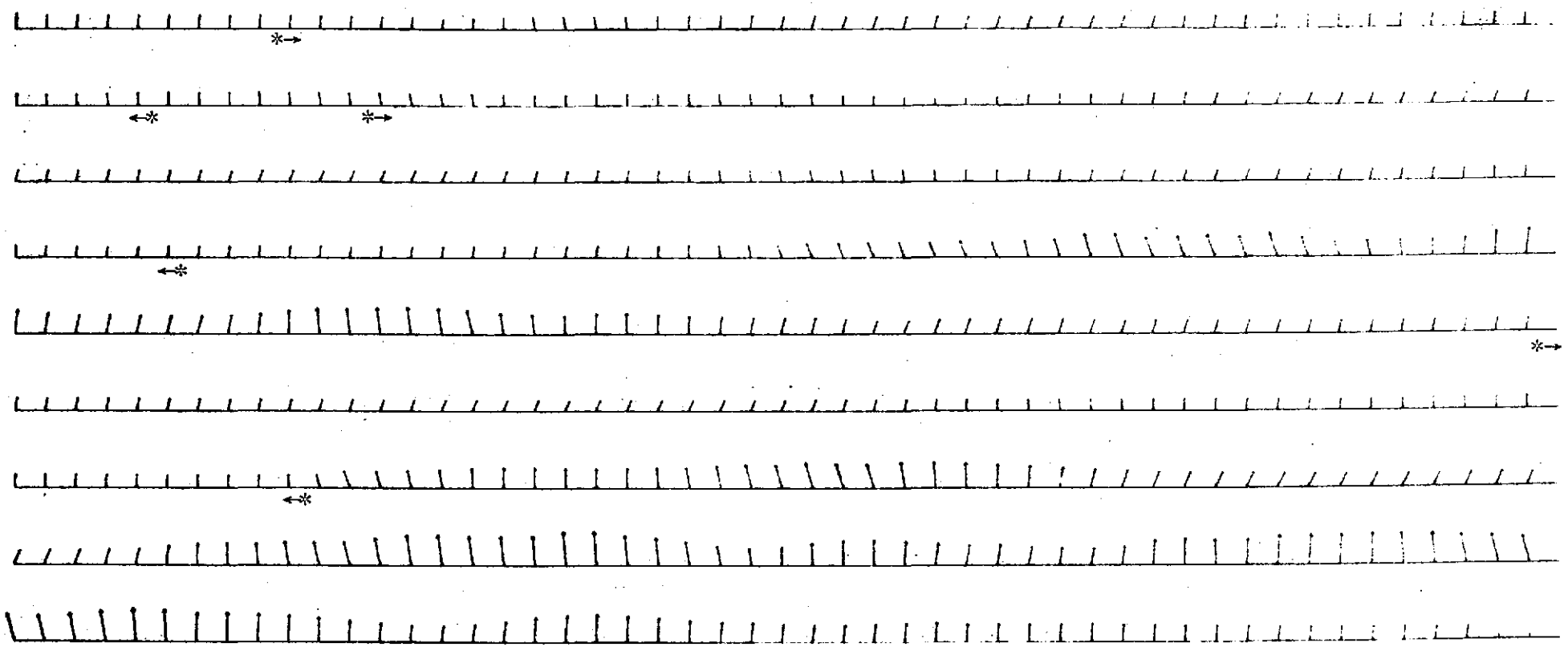

Figure 8. Velocity Vectors for Data Set 3

Note: Each vector is calculated from a pair of voltage readings separated by 65 μsec. There are 260 μsec between each vector. See Table 1 for the statistical evaluation of these data.
Note: The interval designated "1" or "nonvortical" by the appropriate clustering routine is shown by the symbols *→ ←*.

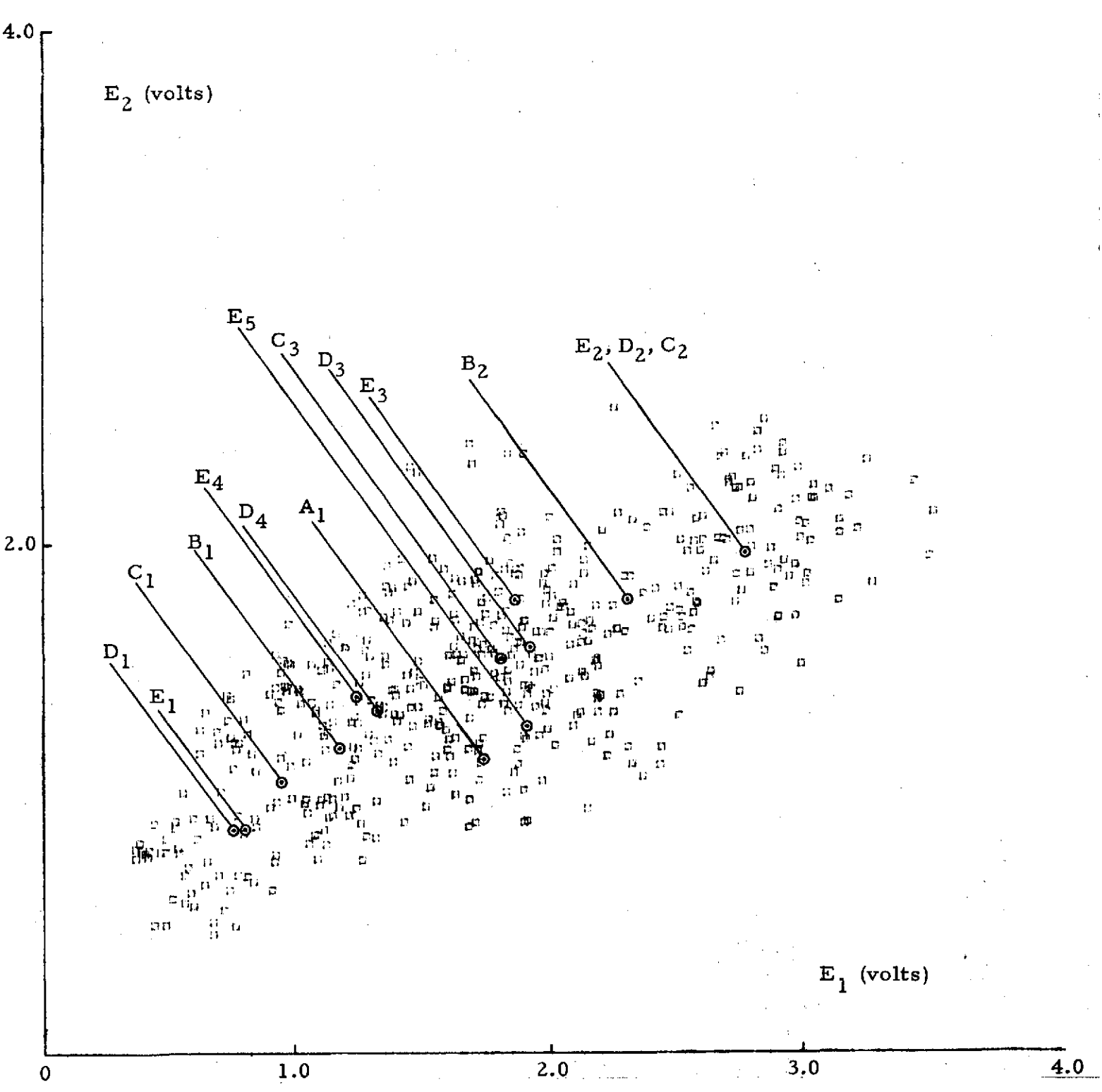

Figure 9. E_1, E_2 voltage pairs for data set No. 1.
(See Table 3 for clustering data.)

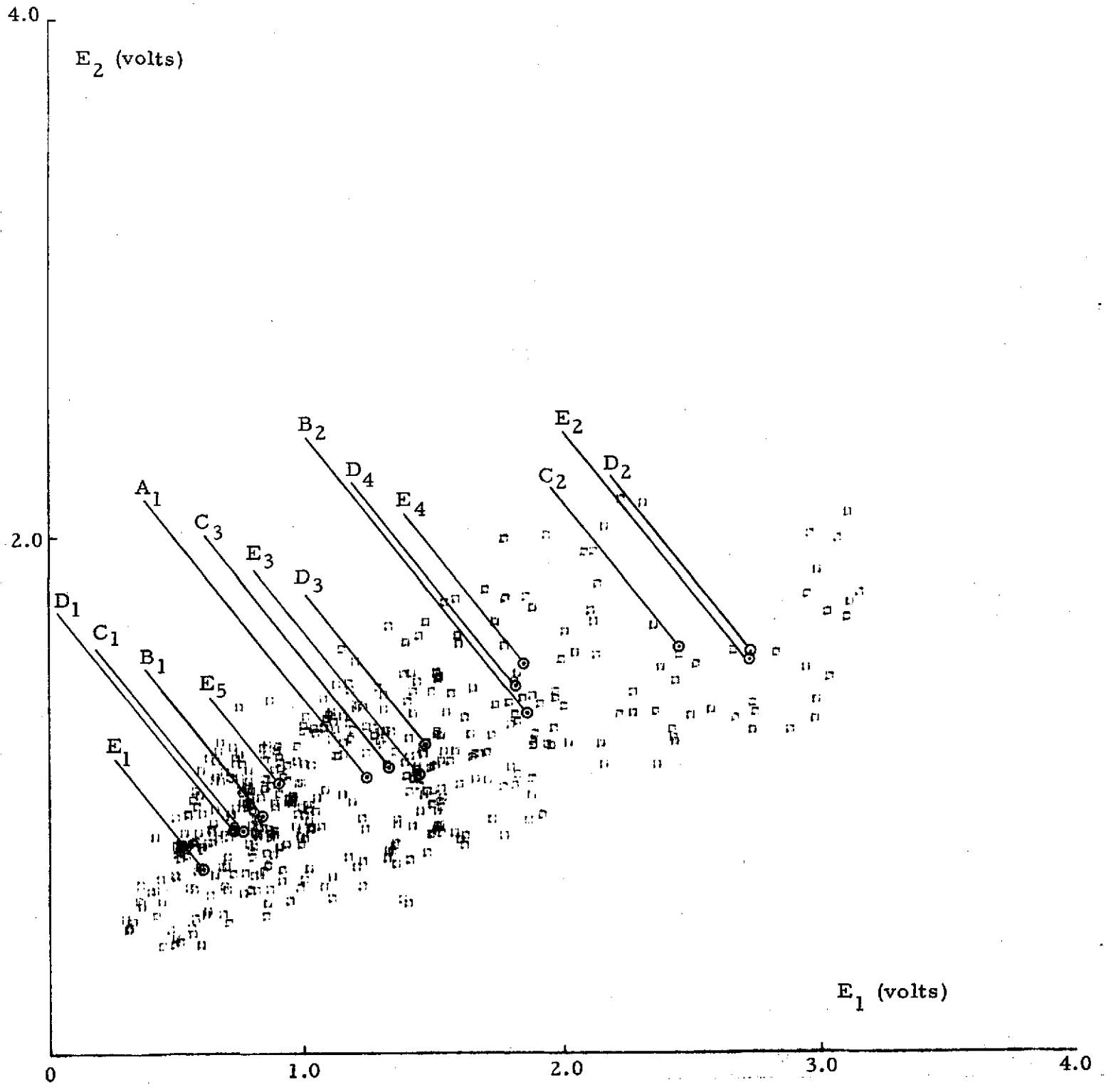

Figure 10. E_1, E_2 voltage pairs for data set No. 2.
(See Table 4 for clustering data.)

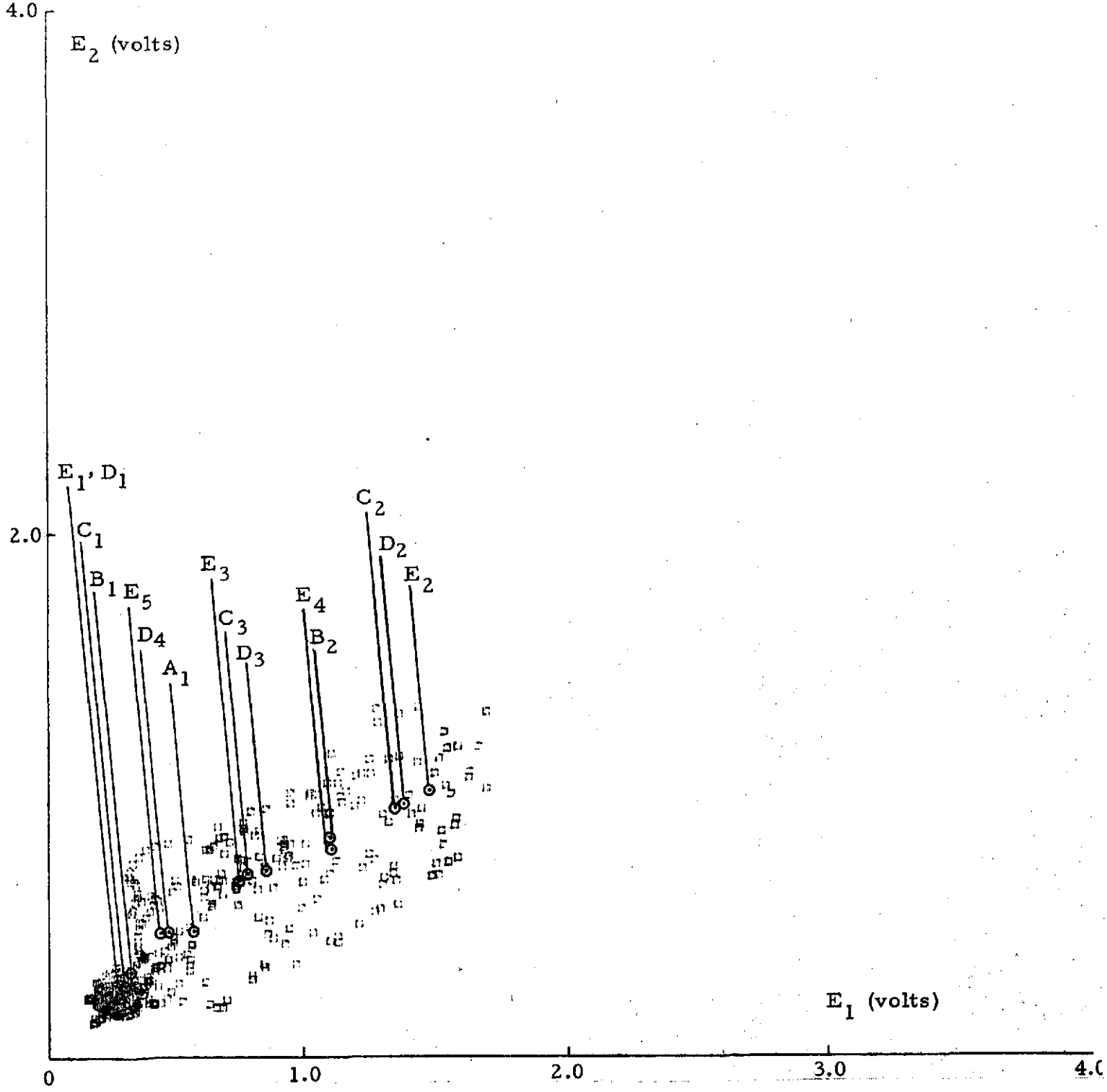

Figure 11. E_1, E_2 voltage pairs for data set No. 3.
(See Table 5 for clustering data.)

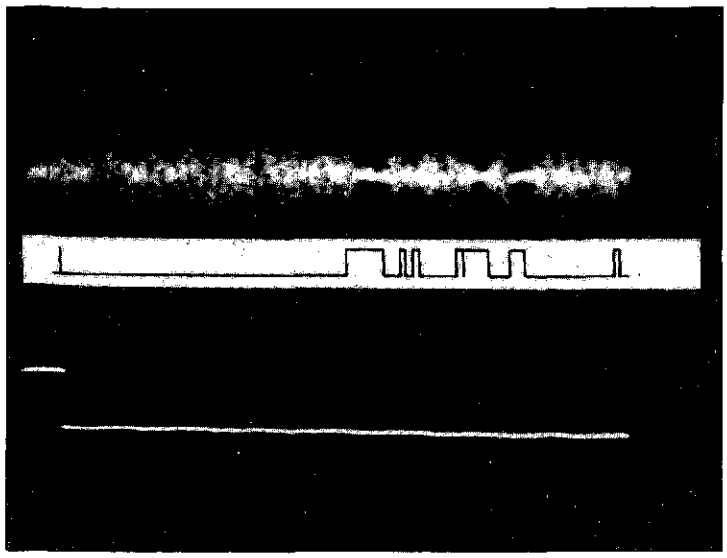

a) Large $\overline{\gamma}$ location in the jet

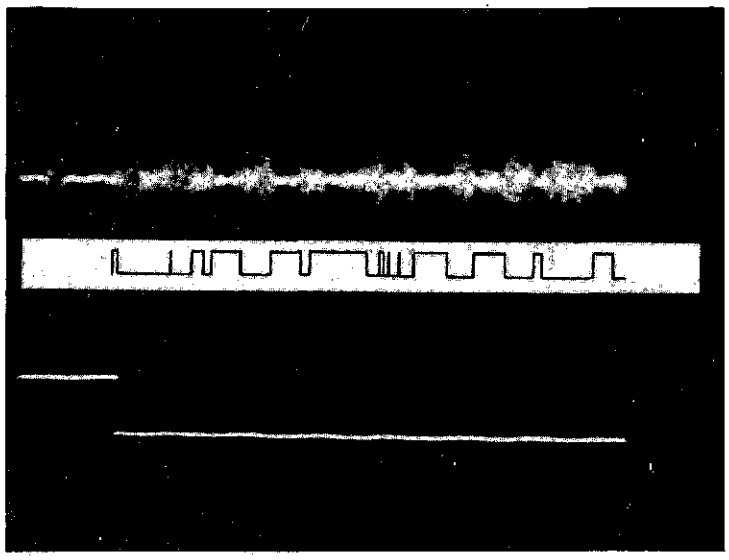

b) Medium $\overline{\gamma}$ location in the jet

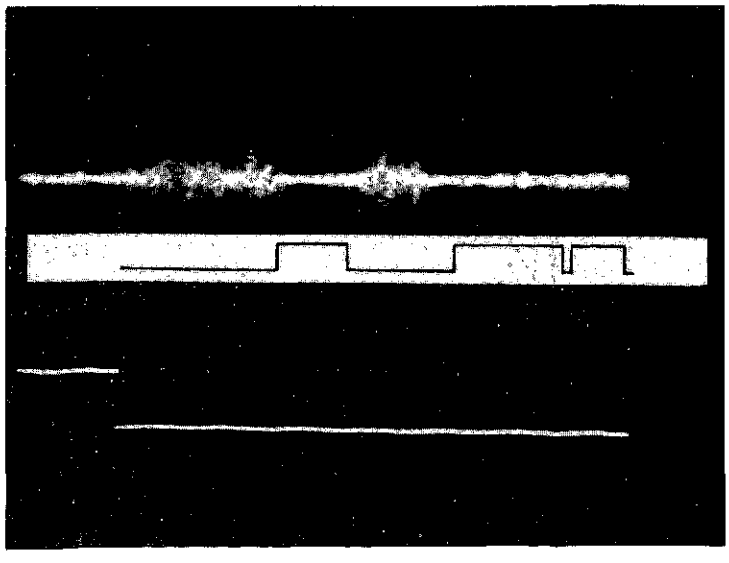

c) Small $\overline{\gamma}$ location in the jet

Figure 12. Oscilloscope trace of the signal $\partial v/\partial t$ compared with the number one cluster grouping. (The upper level of the ink trace signifies the number one cluster. The lower portion of the scope trace signifies the duration of the data acquisition time.)